Chinese Journal of Catalysis 43 (2022) 1945–1954

available at www.sciencedirect.com

ScienceDirect

journal homepage: www.sciencedirect.com/journal/chinese-journal-of-catalysis

Article

Synthesis of mesoporous high-silica zeolite Y and their catalytic cracking performance

Wenhao Cui [a,b,†], Dali Zhu [a,b,†], Juan Tan [c], Nan Chen [a,b], Dong Fan [a], Juan Wang [a], Jingfeng Han [a], Linying Wang [a,*], Peng Tian [a,#], Zhongmin Liu [a]

[a] *National Engineering Laboratory for Methanol to Olefins, Dalian National Laboratory for Clean Energy, Dalian Institute of Chemical Physics, Chinese Academy of Sciences, Dalian 116023, Liaoning, China*

[b] *University of Chinese Academy of Sciences, Chinese Academy of Sciences, Beijing 100049, China*

[c] *Department of Catalysis Chemistry and Engineering, School of Chemical Engineering, Faculty of Chemical, Environmental and Biological Science and Technology, Dalian University of Technology, Dalian 116024, Liaoning, China*

ARTICLE INFO

Article history:
Received 6 December 2021
Accepted 2 March 2022
Available online 20 May 2022

Keywords:
Mesoporous zeolite
FAU
Synthesis
High-silica zeolite Y
Fluid catalytic cracking

ABSTRACT

Mesoporous high-silica zeolite Y with advantages of improved accessibility of acid sites and mass transport properties is highly desired catalytic materials for oil refinery, fine chemistry and emerging biorefinery. Here, we report the direct synthesis of mesoporous high-silica zeolite Y (named MSY, $SiO_2/Al_2O_3 \geq 9.8$) and their excellent catalytic cracking performance. The obtained MSY materials are mesoporous single crystals with octahedral morphology, abundant mesoporosity and excellent (hydro)thermal stability. Both the acid concentration and acid strength of H-form MSY are obviously higher than those of commercial ultra-stable Y (USY), which should be attributed to the uniform Al distribution of MSY zeolite. The H-MSY displays an obviously reduced deactivation rate and improved catalytic activity in the cracking reaction of bulky 1,3,5-triisopropylbenzene (TIPB), as compared with its mesoporogen-free counterpart and USY. In addition, H-MSY was investigated as catalyst for the cracking of industrial heavy oil. The MSY-based catalyst (after aging at 800 °C in 100% steam for 17 h) exhibits superior conversion (7.64% increase) and gasoline yield (16.37% increase) than industrial fluid catalytic cracking (FCC) catalyst under the investigated conditions.

1. Introduction

Zeolites are important crystalline microporous materials, which have been widely applied as catalysts, in particular as solid acid catalysts in industrial processes such as isomerization, Fluid catalytic cracking (FCC), methanol to olefins (MTO), etc. [1–3]. The inherent microporous nature of zeolites (≤ 1 nm) provides unique activity and shape selectivity for catalytic reaction. Unfortunately, it also causes limited access and slow mass transport to/from the active sites within the micropores, restricting the catalytic performance of zeolites. Introducing mesopores into the zeolite crystals has been demonstrated to be an effective way to overcome the problem [4–10], which can effectively ameliorate the diffusion limitation and enhance the catalytic activity, while maintaining the shape selectivity in catalysis.

* Corresponding author. E-mail: lywang@dicp.ac.cn
# Corresponding author. E-mail: tianpeng@dicp.ac.cn
† Contributed equally to this work.

This work was supported by the National Natural Science Foundation of China (21991090, 21991091), the Key Research Program of Frontier Sciences, CAS (QYZDB-SSW-JSC040), and DICP Funding (DICP ZZBS201807).
DOI: 10.1016/S1872-2067(21)64043-3 | http://www.sciencedirect.com/journal/chinese-journal-of-catalysis | Chin. J. Catal., Vol. 43, No. 7, July 2022

Zeolite Y, having three dimensional 12-membered ring channels and spherical supercages, is one of the most important members in zeolite family. Its application in the FCC and hydrocracking processes has brought a revolutionary breakthrough to the petroleum refining industry [11,12]. In recent years, zeolite Y also shows promising catalytic performance for biomass conversion [13–15]. Generally, the primary active component of industrial cracking catalysts is ultra-stable Y (USY) zeolite [16], which is prepared by post-synthesis dealumination with conventional zeolite Y as precursor [17–19]. Although dealumination treatment can enhance the framework SiO_2/Al_2O_3 (SAR) and (hydro)thermal stability, and introduce mesoporosity, it is complex and time-/energy-consuming. Additionally, the formation of dealumination gradient is inevitable, which is unfavorable for catalytic applications [20–22].

Many efforts have been dedicated to the synthesis of mesoporous Y zeolites [23–27]. However, the resultant products have low silica framework and inferior (hydro)thermal stability, restricting their practical application. Direct synthesis of mesoporous high-silica zeolite Y is thus highly attractive, which unfortunately remains a challenge since the first synthesis of zeolite Y in 1960s. Generally, the SAR of zeolite Y synthesized from inorganic systems is limited to be less than 6.5 [28,29]. In 1991, Delprato *et al*. [30] reported that the SAR of zeolite Y can be improved to 9.0 by employing 15-crown-5 ether as an organic structure-directing agent (OSDA). Compared to Na^+ cation, the low charge density of OSDA facilitates the decrease of framework charge density and the improvement of framework SAR. Recently, our group developed a novel NOA-co strategy to realize the direct synthesis of high-silica zeolite Y with tunable SAR up to 15.6 [31]. The novel strategy involves the use of FAU nuclei solution, bulky OSDA (quaternary alkylammonium cations) and low alkalinity gel system. Very recently, during our manuscript preparation, Dusselier *et al*. [32] reported the synthesis of high-silica Y (SAR = 9.6–12.8) by using 15-crown-5 and choline as co-OSDAs. The progress on the direct synthesis of high-silica Y provides chance for the synthesis of their mesoporous counterparts and the investigation of the materials' catalytic performance.

Herein, we report the successful synthesis of mesoporous high-silica zeolite Y (named MSY) and its catalytic performance in hydrocarbon cracking reactions. A facile organosilane surfactant-assisted NOA-co strategy has been developed for the synthesis of MSY materials, which present octahedral morphology with abundant intracrystalline mesoporosity. The characteristics of high-silica framework and mesoporous single-crystal properties endow the MSY materials excellent (hydro)thermal stability. The acidity and catalytic performances of the MSY material are investigated in detail, showing that it has ample acid sites, strong acid strength and superior catalytic activity for cracking of bulky TIPB and industrial heavy oil.

2. Experimental

2.1. Materials

Sodium aluminate (50% Al_2O_3, 39% Na_2O, Shanghai Aladdin Industrial Co.), silica gel (99 wt%, 200–300 mesh Qingdao Macall Group Co.), tetraethyl orthosilicate (TEOS, Shanghai Annaiji Chemical Reagent Co.), sodium hydroxide (NaOH, 99.9 wt%, Shanghai Aladdin Industrial Co.), aluminum isopropoxide (≥ 98 wt%, Shanghai Aladdin Industrial Co.), tetraethylammonium hydroxide (TEAOH, 35 wt% in H_2O, Shanghai Annaiji Chemical Reagent Co.), tetrabutylammonium hydroxide (TBAOH, 40 wt% in H_2O, Shanghai Annaiji Chemical Reagent Co.), [3-(trimethoxysilyl)propyl] octadecyldimethylammonium chloride (TPOAC, 60 wt% in methanol, Shanghai Aladdin Industrial Co.), ammonium chloride (NH_4Cl, 99.5%, Shanghai Aladdin Industrial Co.).

Commercial NaY (named $NaY_{5.6}$, 5.6 refers to the SiO_2/Al_2O_3 ratio detected by XRF) and ultra-stable Y (USY, in NH_4^+ form, SiO_2/Al_2O_3 = 12.9) were used as reference samples. They were purchased from Shanghai Xinnian Petrochemical Additives Co. Ltd.

Protonated form of $NaY_{5.6}$ (H-$Y_{5.6}$) was obtained by ion exchange of NaY three times with 1.0 mol/L NH_4Cl solution (80 °C, 2 h, liquid/solid = 15 mL/g) followed by calcination at 500 °C for 4 h in air. The above procedure was repeated twice. Protonated form of USY was obtained by calcination of NH_4^+-USY at 500 °C for 4 h in air.

2.2. Synthesis of high-silica zeolite Y (named $SY_{9.5}$)

High-silica zeolite Y was hydrothermally prepared using the NOA-co strategy reported by us recently [31]. A FAU nuclei solution (named as solution A) was first prepared from a solution with molar composition of $1SiO_2$:$0.1Al_2O_3$:$0.01Na_2O$:0.12TEAOH:$18.3H_2O$. For details, 6.80 g of aluminum isopropoxide was added into 84.15 g of TEAOH solution and stirred for 60 min to form clear solution. 0.13 g of NaOH was then added and dissolved in the solution. 34.72 g of TEOS was added dropwise into the above solution and stirred for 4 h at room temperature. The obtained clear solution was charged into a Teflon liner of stainless steel autoclave and heated statically at 50 °C for 12 h and then at 100 °C for 48 h. Solution B was prepared as follows: sodium aluminate was added into an aqueous solution containing NaOH under stirring. TBAOH and silica gel were then added in sequence into the solution under stirring to form an initial gel with molar composition of $1SiO_2$:$1/20Al_2O_3$:$0.12Na_2O$:0.2TBAOH:$20H_2O$. Finally, a given amount of solution A was dropped into solution B and aged for 4 h under strong agitation at room temperature to form the final gel. The addition of solution A into the solution B is 10 wt% (based on SiO_2). The final gel was charged into a Teflon liner of 50 mL autoclave. The crystallization was conducted under rotation (30 r/min) at 120 °C for 3.5 d. After crystallization, the solid was collected by filtration, washed with deionized water for three times and then dried in air at 100 °C overnight. The product was named as $SY_{9.5}$, where 9.5 presents the product SiO_2/Al_2O_3 ratio detected by XRF. The as-synthesized sample was calcined in air at 600 °C for 6 h to remove the organic templates. H-form sample was obtained by following steps: ion exchange of the calcined sample three times with

NH_4Cl solution (1.0 mol/L) at 80 °C for 2 h (liquid/solid = 15 mL/g) and calcination in air at 500 °C for 4 h. The Na^+ in the calcined $SY_{9.5}$ was replaced completely after NH_4^+ exchange. The H-form sample was denoted as H-$SY_{9.5}$.

2.3. Synthesis of mesoporous high-silica zeolite Y

The synthesis of mesoporous high-silica zeolite Y is similar to that in part 2.1. The difference lies in the addition of TPOAC in solution B, which was added into the solution after the addition of TBAOH. After stirring for 10 min, silica gel was slowly added into the clear solution under stirring to form a gel with molar composition of $1SiO_2$:$1/xAl_2O_3$:$0.12Na_2O$:0.2TBAOH:$20H_2O$:yTPOAC (x = 20–40, y = 0.005–0.02). The subsequent steps are the same as that in part 2.2.

2.4. Characterization

X-ray powder diffraction (XRD) data were obtained with a PANalytical X'Pert PRO X-ray diffractometer (40 kV, 40 mA) using Cu K_α (λ = 1.54059 Å) radiation. Scanning electron microscopy (SEM) was performed to observe the crystal morphology by using a field emission SEM (Hitachi SU8020). Philips Magix-601 X-ray fluorescence (XRF) spectrometer was used to determine the chemical composition of the samples. The high-resolution transmission electron microscopy (HRTEM) images were performed on a JEM-2100 transmission electron microscope. The temperature-programmed desorption of ammonia (NH_3-TPD) was carried out with Micromeritics Autochem II 2920 analyzer. 200 mg of calcined samples were first outgassed at 600 °C for 1 h under He flow. Then the temperature was decreased to 100 °C and a flow of NH_3/He for 60 min was injected to saturate the sample with NH_3. The samples were purged under He flow until the baseline was stable. The measurement was conducted from 100 to 650 °C (10 °C/min) under 20 mL/min of He flow. N_2 sorption isotherms of the calcined samples were measured on a Micromeritics ASAP 2020 analyzer. Before measurement, the samples (about 100 mg) were pretreated at 350 °C under vacuum for 4 h. FTIR spectra of pyridine adsorption (Py-FTIR) were collected on Thermo Fisher Scientific (IS-50). The samples (about 40 mg) were pressed into a self-supporting wafer with 6 mm in diameter and placed into a quartz cell, which were pretreated at 350 °C for 60 min under vacuum and then cooled down to 100 °C followed by the introduction of pyridine. After desorption at 150 and 300 °C for 1 h, the spectra were collected at RT. Thermal analysis was performed on a TA SDTQ600 analyzer with a heating rate of 10 °C/min in 20 mL/min of air flow. X-ray photoelectron spectrometer (XPS) measurements were performed using a Thermofisher Excalab X+ with Al K_α radiation as the excitation source. The surface charge of the sample was calibrated by referencing to the Al 2p peak to Al_2O_3 and Si 2p peak to SiO_2. ^{13}C CP MAS NMR and ^{29}Si CP MAS NMR were carried out on a Bruker Avance III 600 spectrometer at 150.9 MHz for ^{13}C and 119.2 MHz for ^{29}Si. ^{13}C CP MAS NMR spectrum was measured with a 4 mm MAS probe and a spinning rate of 12 kHz. ^{29}Si CP MAS NMR spectrum was recorded at a spinning rate of 8 kHz using high-power proton decoupling with a π/4 pulse width of 3.6 μs and a recycle delay of 1 s. The ^{29}Si MAS NMR spectra were recorded at a spinning rate of 8 kHz using high-power proton decoupling with a π/4 pulse width of 2.5 μs and a 10 s recycle delay. The Chemical shifts were referenced to Kaolinite at –91.5 ppm. ^{27}Al MAS NMR spectrum was measured at a spinning rate of 12 kHz using one pulse sequence. 200 scans were accumulated with a π/8 pulse width of 0.75 μs and a recycle delay of 2 s. Chemical shifts were referenced to adamantane for ^{13}C, 4,4-dimethyl-4-silapentane sulfonate and sodium salt (DSS) for ^{29}Si and $(NH_4)Al(SO_4)_2{\cdot}12H_2O$ for ^{27}Al.

2.5. Catalytic tests

N-octane cracking was tested in a fixed-bed quartz tubular reactor (8 mm inner diameter) at atmospheric pressure. The catalyst (100 mg, 40–60 mesh) was first dehydrated in 40 mL/min of N_2 at 500 °C for 0.5 h. The temperature was then reduced to 460 °C in N_2. N-octane was fed by passing N_2 flow (40 mL/min) through a saturator containing n-octane at 20 °C. An online Agilent 7890A GC equipped with a PONA capillary column and an FID detector was used to analyze the effluents. The effluents from the reactor were kept at 200 °C.

1,3,5-Triisopropylbenzene (TIPB) cracking was conducted using same reactor as n-octane cracking. For each test, 50 mg of catalyst (40–60 mesh) diluted by 0.50 g quartz was used, which was dehydrated in N_2 (40 mL/min) at 550 °C for 40 min before the reaction. The temperature was then reduced to 200 °C in N_2. TIPB was fed by passing N_2 flow (100 mL/min) through a saturator containing TIPB at 80 °C. An online Agilent 7890A GC equipped with a PONA capillary column and an FID detector. The effluents from the reactor were kept at 200 °C.

For catalytic cracking of heavy oil, a fixed-bed stainless steel reactor with catalyst loading of 4 g (20–40 mesh) was used. The properties of the heavy oil used are given in Table S1. The cracking reaction was operated at 482 °C with a reaction time of 75 s. The total amount of heavy oil feeded was 1.33 g. The gas products and liquid products were collected separately and analyzed by gas chromatographs with FID detectors using a TDX-1 packed column and a PoraPLOT Q capillary column, respectively. The retention time of n-dodecane (216 °C) was taken as the boundary of gasoline and diesel. N-dodecane was included into gasoline. The coke on the spent catalysts was measured by TG. For the preparation of zeolitic catalyst, the as-synthesized MSY zeolite was first calcined at 600 °C for 3 h, and then ion exchanged with 1 mol/L $LaCl_3{\cdot}7H_2O$ solution at 50 °C for 2 h (solid/liquid = 5 g/100 mL) followed by filtration, washing and drying at 120 °C. La-modified MSY zeolite (35 wt%) was dispersed into a slurry of alumina sol (20 wt%) and clay (45 wt%), after calcination at 600 °C for 3 h. The mixture was dried at 120 °C for 12 h and calcined for 1 h at 500 °C. The resultant catalyst has a loading of 1.3 wt% La detected by XRF.

3. Results and discussion

3.1. Synthesis, morphology and textural properties of mesoporous high-silica zeolite Y

Table 1
Synthesis conditions, product phases, compositions and textural properties of the high-silica zeolite Y samples.

Sample	Starting gel [a]			Product		Surface area [c] (m^2/g)			Pore volume [c] (cm^3/g)		Relative crystallinity % [e]
	x	*y*	Time (day)	Phase	SAR [b]	S_{BET}	S_{micro}	S_{exter}	V_{micro}	V_{meso}	
$SY_{9.5}$	20	0	3.5	FAU	9.5 (10.0) [9.8]	644	585	59	0.27	0.06	100
1	20	0.005	3.5	FAU	9.8	692	567	125	0.26	0.13	94.9
2	20	0.01	3.8	FAU	10.2	702	524	178	0.27	0.16	85.1
3 ($MSY_{10.7}$)	20	0.015	4.5	FAU	10.7 (9.4) [10.7]	779	568	211	0.26	0.22	84.8
4	20	0.02	5.2	FAU+β (trace)	11.3	770	570	200	0.27	0.18	128.3
5	30	0.01	5.4	FAU	12.6	770	587	183	0.27	0.17	125.1
6[d]	40	0.01	8.0	FAU+β+ MOR	17.5	—	—	—	—	—	—
USY	—	—	—	FAU	12.9 (8.1) [17.2]	632	537	95	0.25	0.14	98.8
$NaY_{5.6}$	—	—	—	FAU	5.6	540	504	36	0.24	0.03	68.1

[a] Initial gel: $1SiO_2$:$1/xAl_2O_3$:$0.12Na_2O$:0.20TBAOH:yTPOAC:$20H_2O$; The addition of nuclei solution into the initial gel is 10 wt% (based on SiO_2). The final gel is crystallized at 120 °C.
[b] Bulk SAR(SiO_2/Al_2O_3) measured by XRF. The value in the bracket is surface SAR measured by XPS. The value in square bracket is framework SAR calculated according to ^{29}Si MAS NMR. As-synthesized samples were used for the measurements.
[c] S_{BET}: BET surface area; S_{micro}: *t*-Plot micropore surface area; S_{exter} (external surface area) = S_{BET} – S_{micro}; V_{micro}: *t*-plot micropore volume; V_{meso} = V_{total} – V_{micro}, V_{total} is evaluated at P/P_0 = 0.99.
[d] Na_2O/SiO_2 in the initial gel is changed to 0.11.
[e] The relative crystallinity was calculated based on the areas of the eight peaks at 10.3°, 12.1°, 16.0°, 19.1°, 20.8°, 24.2°, 27.6° and 31.9° by using $SY_{9.5}$ as standard sample.

Direct synthesis of mesoporous high-silica zeolite Y was carried out by a TPOAC-assisted NOA-co strategy. It is noted that the addition sequence of TPOAC mesoporogen during the initial gel preparation is crucial for achieving a pure FAU-type product. Fig. S1 displays the different addition sequences of TPOAC and the SEM images of the products. It is clear that only procedure B with the addition of TPOAC between TBAOH and silica gel can lead to highly pure product. Likely, the longer crystallization times required for complete crystallization of Procedure A, C and D cause the formation of impurities. Therefore, the synthesis investigation was carried out based on procedure B. The detailed synthetic conditions, product phases and product SAR are summarized in Table 1. For comparison, the synthesis under similar conditions without the addition of TPOAC is also conducted (sample $SY_{9.5}$ in Table 1).

Fig. 1(a) displays the XRD patterns of samples $MSY_{10.7}$ and $SY_{9.5}$, which present the characteristic diffraction peaks of FAU-type zeolite and evidence the phase purity of the samples. The SEM images of $MSY_{10.7}$ crystals are shown in Figs. 1(b)–(d), which present typical octahedral morphology in sizes of 50–250 nm. Further magnification reveals that the surface of $MSY_{10.7}$ crystals is rather rough with sponge-like appearance, distinct from the smooth surface of $SY_{9.5}$ crystals (Fig. S2). Moreover, the product compositions listed in Table 1 indicate that the framework SARs of $MSY_{10.7}$ and $SY_{9.5}$ were close to their values measured by XRF. Moreover, the as-synthesized $MSY_{10.7}$ possesses higher framework SAR than $SY_{9.5}$, which suggests the incorporation of TPOAC into the framework.

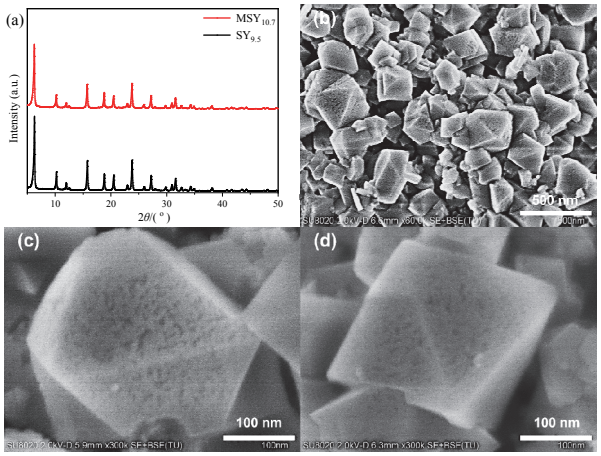

Fig. 1. (a) XRD patterns of the as-synthesized $MSY_{10.7}$ and $SY_{9.5}$. (b) SEM images of $MSY_{10.7}$. (c,d) High-magnification SEM images to show the surface of $MSY_{10.7}$ crystals.

N_2 sorption isotherms of the samples and the corresponding BJH pore size distribution (PSD) based on the adsorption branch are depicted in Fig. 2. Sample $SY_{9.5}$ presents a type-I isotherm with an inconspicuous hysteresis loop in the P/P_0 range of 0.4–1.0. The absence of mesopores in the PSD curve suggests the pure micropore characteristic of $SY_{9.5}$. Sample $MSY_{10.7}$ shows a type (I+IV) isotherm with two obvious absorption increase and small hysteresis loops in the P/P_0 region of 0.3–0.6 and 0.8–1.0. The corresponding PSD curve evidences the existence of mesopores centered at 2.5–7 nm, consistent with the pore sizes on the crystal surface observed by high-resolution SEM images (Fig. 1). The textural properties of the samples are listed in Table 1. The micropore volume and micropore surface area of $MSY_{10.7}$ are close to those of $SY_{9.5}$, confirming its good crystallinity. The external surface area and mesopore volume of $MSY_{10.7}$ are 211 m^2/g and 0.22 cm^3/g, respectively. Both values are about 3.6 times higher than those of $SY_{9.5}$.

Fig. 3 displays the TEM images of sample $MSY_{10.7}$. Abundant mesopores can be observed under low magnification (Figs. 3(a) and 3(c)). The selected area electron diffraction (SAED) pattern of $MSY_{10.7}$ particle is given in Fig. 3(b). The highly discrete diffraction spots evidence the single crystal nature of the sample.

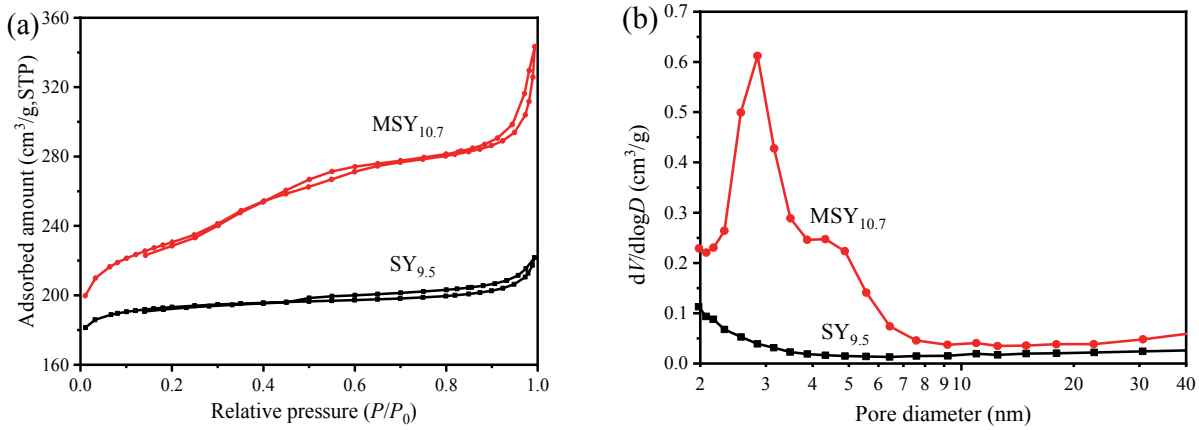

Fig. 2. N_2 sorption isotherms (a) and BJH pore size distribution curves (b) of the samples.

Fig. 3(d) present the high-resolution image of the selected region in Fig. 3(c). Irregular mesopores in sizes of 3–10 nm could be clearly discerned, which interrupt the ordered microporous structures with clear fringe spacing. More importantly, most of the mesopores show good connectivity with the crystal surface, which would be favorable for the improvement of mass transport and the enhancement of catalytic performance, especially for the reactions involving bulky molecules. These results agree well with the textural characteristics from N_2 physisorption.

Both the mesoporosity and phase purity of mesoporous high-silica zeolite Y were found to be affected by the usage of TPOAC in the initial gel (Table 1 and Fig. S5). The SEM images and XRD patterns of the products synthesized with varied TPOAC/SiO_2 ratios are shown in Figs. S3 and S4, respectively. For the synthesis system with gel SAR of 20, when TPOAC/SiO_2 < 0.02, the increasing TPOAC amount shows a positive effect on the enhancement of external surface area and mesoporous volume of the products (samples 1, 2 and $MSY_{10.7}$). However, more TPOAC addition would cause the appearance of trace Beta impurity (sample 4, Fig. S4). The corresponding product SAR displays a rising trend with the incremental usage of TPOAC, which confirms the introduction of TPOAC into the framework acting as both mesoporogen and part of silica source. Moreover, XPS analyses reveal that the surface SAR (9.4) of $MSY_{10.7}$ is close to the bulk. The homogeneous elemental distribution in the crystals implies that the Si atoms of TPOAC are involved in the crystal growth homogeneously, instead of congregating on the external surface. For the system with higher gel SAR of 30, the resultant product (sample 5) presents good purity, improved SAR and similar textural properties when compared with sample 2 (both samples have the same usage of mesoporogen, TPOAC/SiO_2 = 0.01). Further increasing the gel SAR to 40, the product, however, is contaminated by impurities together with obviously reduced crystallization rate (sample 6, Figs. S3 and S4).

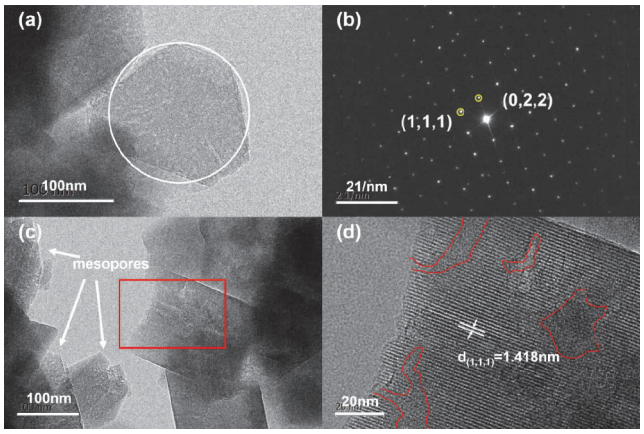

Fig. 3. TEM images and SAED pattern of the mesoporous high-silica zeolite Y (sample $MSY_{10.7}$). (a,c) Low magnification images. (b) SAED pattern taken from selected circle region in (a). (d) High-resolution image corresponds to the rectangle region in (c).

3.2. *Solid-state NMR characterization*

^{13}C CP MAS NMR spectra were measured to learn the status of OSDA species and the TPOAC in the samples. As shown in Fig. 4(a), the signals ascribed to TEA^+ and TBA^+ can be clearly identified, evidencing their coexistence in $MSY_{10.7}$ [31]. In addition, compared to the spectrum of $SY_{9.5}$, extra strong signal at 30.8 ppm can be observed for $MSY_{10.7}$, which should arise from the methylene moieties in the long-alkyl chain of TPOAC [33,34]. Other carbon species of TPOAC, some of which overlap with those of TEA^+ and TBA^+, are also labeled in the spectrum. These results demonstrate that the organic part of TPOAC has been incorporated into the crystals [33,34].

The ^{29}Si CP MAS NMR spectra are illustrated in Fig. 4(b). The sharp resonance peaks centered at –107 and –102 ppm were ascribed to $Si(OSi)_4$ and $Si(OAl)(OSi)_3$ respectively. The smaller peak at –95 ppm was attributed to $Si(OAl)_2(OSi)_2$. The similar Si species distribution of $MSY_{10.7}$ and $SY_{9.5}$ suggests that the addition of TPOAC didn't alter the chemical environments of Si atoms. In addition, the signal at -66 ppm associated with the Si atoms of TPOAC ($RSi(OAl)_n(OH)_{3-n}$) is inconspicuous in the spectrum of $MSY_{10.7}$ [35,36]. This might be due to the low addition amount of TPOAC (0.015) or/and its full condensation with the framework (n = 3). The ^{27}Al MAS NMR spectrum of the as-synthesized $MSY_{10.7}$ (Fig. S6) only shows one strong reso-

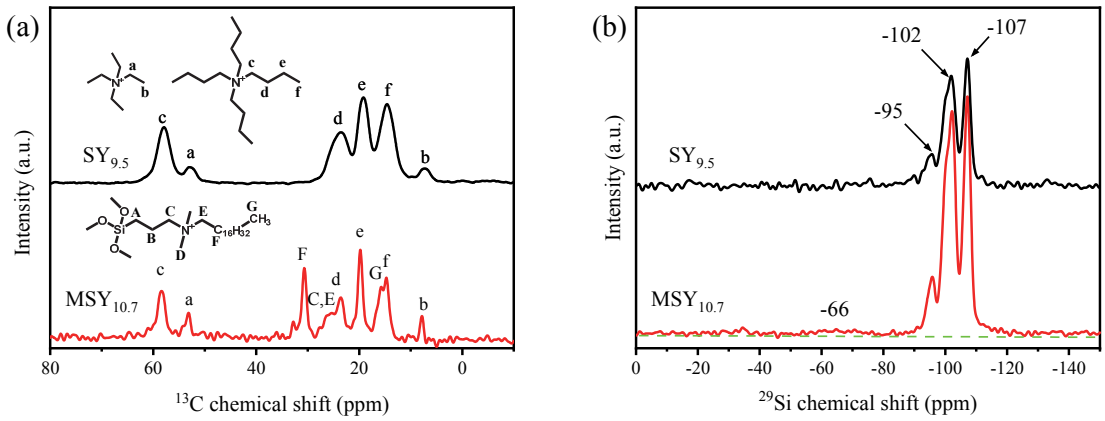

Fig. 4. ^{13}C CP MAS NMR (a) and ^{29}Si CP MAS NMR (b) spectra of the as-synthesized high-silica zeolite Y.

nance around 60 ppm, evidencing the tetrahedral Al species in the framework of mesoporous high-silica product.

3.3. Thermal and hydrothermal stability

Thermal and hydrothermal stability is important for the materials' practical applications. The TG-DSC profiles are presented in Figs. 5(a) and 5(b). With the increase of TPOAC addition, the MSY samples show a gradually increased weight loss in the range of 120–700 °C, and one extra exothermal peak at about 301 °C in the DSC curves becomes evident (associated with the combustion decomposition of long-alkyl chain in TPOAC [37]). These are clear evidence for the existence of TPOAC and consistent with the above characterization results. Moreover, all samples show a structural collapse temperature around 1050–1080 °C in the DSC curves, demonstrating their good thermal stability.

H-form $MSY_{10.7}$ instead of Na-form sample was used to investigate the hydrothermal stability, as the existence of Na^+ may fasten the structural deterioration under high-temperature steam condition [38]. Conventional $H\text{-}Y_{5.6}$ and $H\text{-}SY_{9.5}$ were employed as reference samples. From Fig. 5(c), mesoporous $H\text{-}MSY_{10.7}$ possesses superior hydrothermal stability than $H\text{-}Y_{5.6}$. Its micropore volume retention after steam treatment is comparable with that of $H\text{-}SY_{9.5}$ sample. Previous works have demonstrated that mesoporous zeolites in single crystal nature can help achieve better hydrothermal stability due to the relatively high integrity of microporous structures [39,40]. Herein, the excellent hydrothermal stability of MSY is thus ascribed to its high framework SAR and single crystal nature.

3.4. Acidity

NH_3-TPD was employed to examine the acidic properties of $H\text{-}MSY_{10.7}$. Moreover, $SY_{9.5}$ and commercial USY (Fig. S7) were measured as reference samples. As displayed in Fig. 6(a), all samples present two desorption peaks at 150–300 and 350–550 °C, which correspond to the weak and strong acid sites, respectively [28]. Compared with commercial H-USY, $H\text{-}MSY_{10.7}$ possesses obviously large acid amount and high acid strength. It is speculated that the relatively low structural integrity due to dealumination treatment and ununiform Al distribution in H-USY (see XPS results in Table 1) caused its inferior acidity. On the other hand, the acid concentration of $H\text{-}MSY_{10.7}$ is lower than that of mesoporogen-free synthesized $H\text{-}SY_{9.5}$. This is indeed a common phenomenon for mesoporous zeolites [22,25,26,41–43] and may be caused by the lower

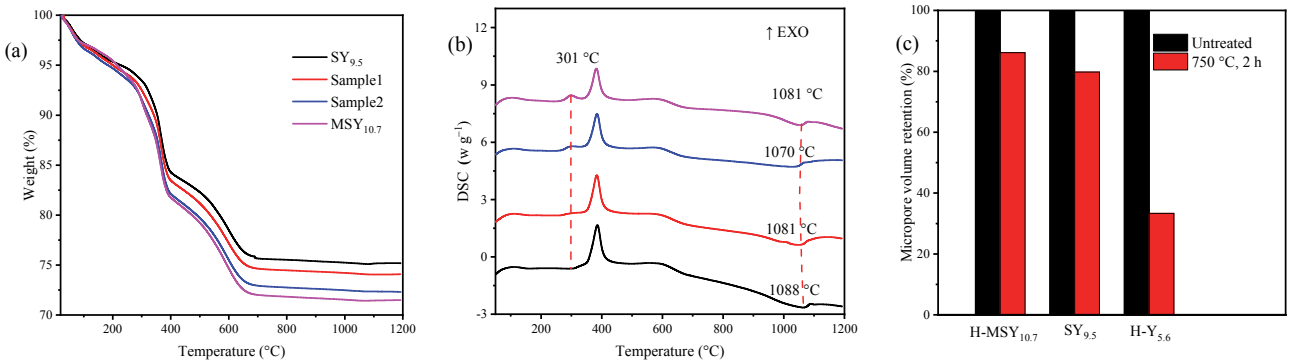

Fig. 5. Thermal and hydrothermal stability of the samples. TG (a) and DSC (b) curves of the as-synthesized high-silica zeolite Y. (c) The micropore volume retention of H-form samples after hydrothermal treatment. The micropore volume of each fresh sample is defined as 100%.

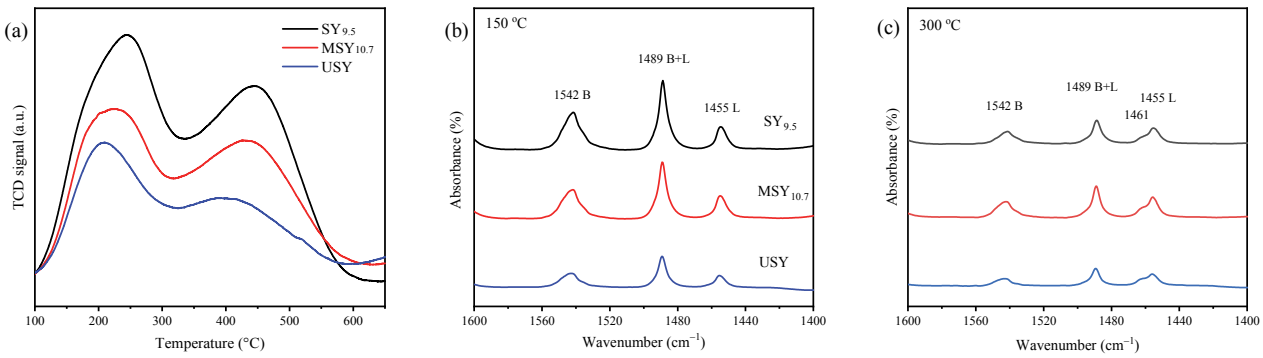

Fig. 6. Acidity of the H-form high-silica zeolite Y. (a) NH_3-TPD profiles. (b,c) FTIR spectra of pyridine ring-related vibration regions on the H-form samples after pyridine desorption at 150 and 300 °C.

crystallinity and relatively serious dealumination during calcination process.

Py-FTIR spectra were also recorded to study the acid strength and types of the samples (Figs. 6(b) and 6(c)). The peaks at 1542 and 1455 cm^{-1} are related to the Brønsted acid sites (BAS) and Lewis acid sites (LAS) respectively, and the peak at 1489 cm^{-1} is associated with both BAS and LAS [32,44]. Moreover, after pyridine desorption at 300 °C, a new weak band at 1461 cm^{-1} can be observed, which may arise from a complex between pyridine and tricoordinated aluminum [45–47]. The qualitative results are shown in Table 2, which reveals that the total acid sites decrease in an order of H-$SY_{9.5}$ > H-$MSY_{10.7}$ > H-USY, in agreement with the NH_3-TPD results. Compared with H-$SY_{9.5}$, H-$MSY_{10.7}$ possesses relatively low BAS, but comparable LAS. Both the BAS and LAS on H-USY are obviously lower than those on H-$MSY_{10.7}$ and H-$SY_{9.5}$. After pyridine desorption at 300 °C, the amount of BAS shows a bigger decrease than that of LAS for all three samples, indicating the increased proportion of LAS in strong acid sites.

To better understand the variation of the acid concentration, the framework SAR of H-form samples was calculated according to ^{29}Si MAS NMR and the results are listed in Table 2. All three samples show higher framework SAR than their as-synthesized counterparts, implying the occurrence of dealumination. The framework SAR of the H-form samples presents an increased sequence of H-$SY_{9.5}$ < H-$MSY_{10.7}$ < H-USY. Especially for H-USY, its framework SAR reaches as high as 20.9, which suggests its lower stability of framework Al atoms.

Table 2
Framework SAR of the H-form samples and the amounts of Brønsted and Lewis acid sites determined by FT-IR spectra of pyridine adsorption at 150 °C [a].

Sample	SAR [b]	BAS (mmol/g)	LAS (mmol/g)	BAS+LAS (mmol/g)	BAS/LAS
H-$SY_{9.5}$	11.9	0.90	0.26	1.16	3.53
H-$MSY_{10.7}$	13.6	0.70	0.26	0.97	2.71
H-USY	20.9	0.30	0.11	0.41	2.88

[a] The data are calculated by employing molar extinction coefficients from the literature [44] (ε(B) = 1.67 cm μmol^{-1} and ε(L) = 2.22 cm μmol^{-1}).
[b] Framework SAR calculated according to ^{29}Si MAS NMR.

The framework SARs of the samples are in consistence with the amounts of BAS measured by pyridine-adsorbed FT-IR.

3.5. Catalytic performance

N-octane and TIPB cracking were selected as model reactions to test the catalytic performance of H-$MSY_{10.7}$. As the kinetic diameter of linear n-octane (0.63 nm) is smaller than the micropore size of zeolite Y (0.74 nm), n-octane molecules can diffuse into the supercages of zeolite Y and contact all the acid sites of the catalysts. From Fig. 7(a), all three catalysts suffer a fast deactivation with time on stream, and the catalytic activities are essentially proportional to their acid amounts. To better understand the phenomenon, the zero length column (ZLC) experiments were carried out to measure the diffusion coefficients of n-octane in H-$MSY_{10.7}$ and H-$SY_{9.5}$. As shown in Fig. S8, the pore diffusivity (D/r^2) of H-$MSY_{10.7}$, calculated based on the ZLC model [48], is about twice higher than that of H-$SY_{9.5}$. This implies that transport resistance of n-octane in H-$MSY_{10.7}$ is weaker than in H-$SY_{9.5}$, consistent with the abundant mesoporosity of H-$MSY_{10.7}$. Therefore, it is speculated that the acidity played the dominant role for the cracking activity of n-octane on zeolite Y.

Fig. 7(b) illustrates the TIPB cracking results of the catalysts. It is noted that the cracking activity of TIPB is closely related with the acid sites on the external surface of zeolite Y due to its large kinetic diameter (0.95 nm). Mesoporous H-$MSY_{10.7}$ presents the slowest deactivation rate and high catalytic activity among the catalysts. Also, H-$MSY_{10.7}$ exhibits the highest cracking depth as evidenced from the product yields listed in Table S2. It is believed that the largest external surface area, stronger acidity and larger acid amounts work together and contribute to the superior catalytic activity of H-$MSY_{10.7}$.

Heavy oil cracking was further carried out to learn the catalytic performance of mesoporous high-silica zeolite Y for industrial feedstock. The properties of heavy oil feedstock are shown in Table S1. For comparison, industrial FCC catalyst was used as a reference. Both catalysts were hydrothermally aged at 800 °C (100% steam) for 17 h prior to the cracking reaction. The reaction results are listed in Table 3. Remarkably, $MSY_{10.7}$-based catalyst presents superior heavy oil conversion

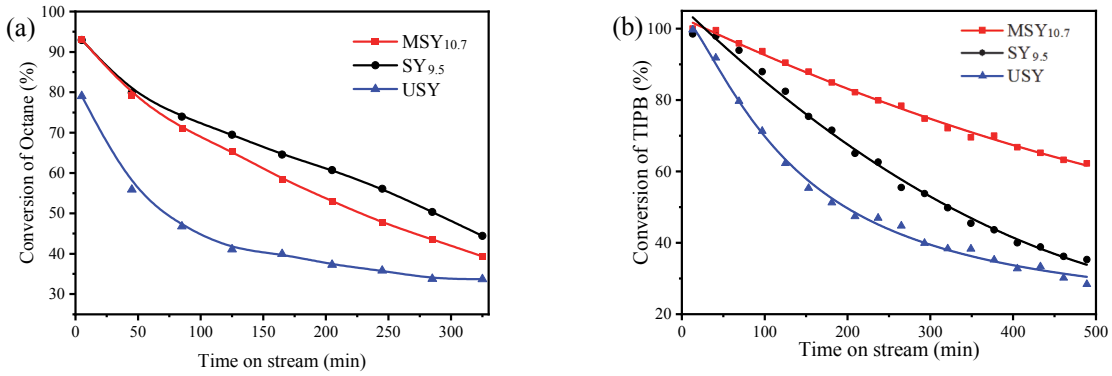

Fig. 7. Catalytic cracking performance of the H-form high-silica zeolite Y. (a) N-octane cracking versus time on stream. Reaction conditions: T = 460 °C, $WHSV_{n\text{-}octane}$ = 3.88 h^{-1}. (b) TIPB cracking versus time on stream. Reaction conditions: T = 200 °C, $WHSV_{TIPB}$ = 3.08 h^{-1}.

(93.11%) than industrial catalyst (85.47%). The gasoline yield (61.46%) on the former is also amazing, which is 16.37% higher than the latter. Although higher LPG yield is observed for industrial catalyst (containing small amount of ZSM-5), the total yield of (LPG + gasoline + diesel) on $MSY_{10.7}$-based catalyst is 7 wt% higher than on industrial FCC catalyst. More importantly, the high cracking activity of $MSY_{10.7}$-based catalyst didn't cause excess coke deposition. The coke amount on it is 5.42%, only slightly higher than on industrial catalyst (4.59%). These results demonstrate the superior catalytic cracking performance of mesoporous high-silica zeolite Y for heavy oil. This would be highly valuable for the industrial (hydro)cracking processes with increasing tendency of heavy feedstocks.

4. Conclusions

Mesoporous high-silica zeolite Y with abundant intracrystalline mesoporosity, uniform Al distribution, and excellent (hydro)thermal stability has been synthesized by TPOAC-assisted NOA-co strategy. The H-MSY zeolite has larger acid concentration and stronger acid strength than commercial USY, which help the material exhibit good catalytic activity in the cracking of bulky TIPB with slow deactivation rate, high activity and cracking depth. More importantly, $MSY_{10.7}$-based catalyst after 800 °C hydrothermal aging treatment displays superior conversion and gasoline yield than industrial FCC catalyst for the cracking of heavy oil, which is valuable for the industrial (hydro)cracking processes with increasing tendency of heavy feedstocks. Besides as FCC catalysts, MSY zeolite is also expected to facilitate a wide variety of reactions where mass transport is a limiting factor, such as hydrocracking and biomass conversion.

Table 3
Heavy oil cracking on $MSY_{10.7}$-based catalyst and industrial FCC catalyst.

Items (wt%)	$MSY_{10.7}$-based catalyst	Industrial FCC catalyst
Conversion	93.11	85.47
Dry gas	1.02	1.23
Gasoline	61.46	45.09
Diesel	13.07	14.14
Gasoline + Diesel	74.53	59.23
Diesel/Gasoline ratio	0.21	0.31
Liquid petroleum gas (LPG)	12.13	20.41
LPG+Gasoline+Diesel	86.66	79.64
Heavy oil	6.89	14.53
Coke	5.42	4.59

Author Contributions

All authors contributed to this work. All authors have given approval to the final version of the paper.

Declaration of Competing Interest

The authors declare no competing financial interest.

Electronic supporting information

Supporting information is available in the online version of this article.

References

[1] J. Shi, Y. D. Wang, W. M. Yang, Y. Tang, Z. K. Xie, *Chem. Soc. Rev.*, **2015**, 44, 8877–8903.
[2] A. Corma, *Chem. Rev.*, **1995**, 95, 559–614.
[3] Y. Li, J. H. Yu, *Nat. Rev. Mater.*, **2021**, 6, 1156–1174.
[4] K. Egeblad, C. H. Christensen, M. Kustova, C. H. Christensen, *Chem. Mater.*, **2008**, 20, 946–960.
[5] J. Perez-Ramirez, C. H. Christensen, K. Egeblad, C. H. Christensen, J. C. Groen, *Chem. Soc. Rev.*, **2008**, 37, 2530–2542.
[6] A. Sachse, J. Garcia-Martinez, *Chem. Mater.*, **2017**, 29, 3827–3853.
[7] X. J. Meng, F. Nawaz, F. S. Xiao, *Nano Today*, **2009**, 4, 292–301.
[8] D. Kerstens, B. Smeyers, J. Van Waeyenberg, Q. Zhang, J. H. Yu, B. F. Sels, *Adv. Mater.*, **2020**, 32, 2004690.
[9] M. Hartmann, M. Thommes, W. Schwieger, *Adv. Mater. Interfaces*, **2021**, 8, 2001841.
[10] D. Verboekend, J. Perez-Ramirez, *Catal. Sci. Technol.*, **2011**, 1, 879–890.
[11] J. Garcia-Martinez, K. Li, G. Krishnaiah, *Chem. Commun.*, **2012**, 48, 11841–11843.

Graphical Abstract

Chin. J. Catal., 2022, 43: 1945–1954 doi: 10.1016/S1872-2067(21)64043-3

Synthesis of mesoporous high-silica zeolite Y and their catalytic cracking performance

Wenhao Cui, Dali Zhu, Juan Tan, Nan Chen, Dong Fan, Juan Wang, Jingfeng Han, Linying Wang *, Peng Tian *, Zhongmin Liu
Dalian Institute of Chemical Physics, Chinese Academy of Sciences;
University of Chinese Academy of Sciences;
Dalian University of Technology

Mesoporous high-silica zeolite Y with high (hydro)thermal stability has been successfully synthesized, which possesses larger acid concentration and stronger acid strength than USY, and exhibits superior catalytic performance in the cracking of hydrocarbons and industrial heavy oil.

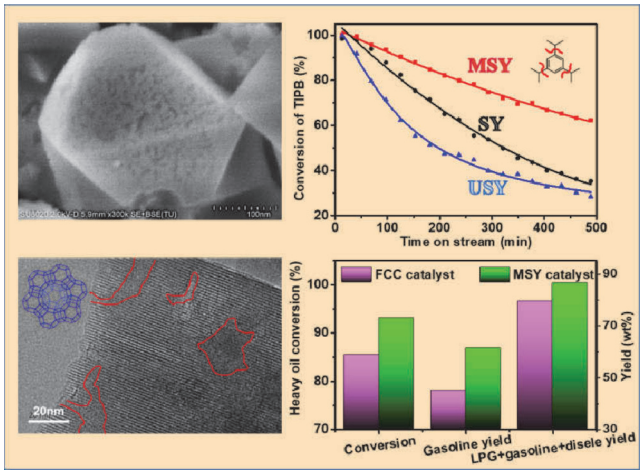

[12] E. T. C. Vogt, B. M. Weckhuysen, *Chem. Soc. Rev.*, **2015**, 44, 7342–7370.
[13] J. He, Z. J. Wu, Q. Q. Gu, Y. S. Liu, S. Q. Chu, S. H. Chen, Y. F. Zhang, B. Yang, T. H. Chen, A. Q. Wang, B. M. Weckhuysen, T. Zhang, W. H. Luo, *Angew. Chem. Int. Ed.*, **2021**, 60, 23713–23721.
[14] Z. Jin, X. F. Yi, L. Wang, S. D. Xu, C. T. Wang, Q. M. Wu, L. X. Wang, A. N. Zheng, F. S. Xiao, *Appl. Catal. B*, **2019**, 254, 560–568.
[15] T. Iida, M. Shetty, K. Murugappan, Z. S. Wang, K. Ohara, T. Wakihara, Y. Roman-Leshkov, *ACS Catal.*, **2017**, 7, 8147–8151.
[16] R. H. Harding, A. W. Peters, J. R. D. Nee, *Appl. Catal. A*, **2001**, 221, 389–396.
[17] P. Peng, X.-H. Gao, Z.-F. Yan, S. Mintova, *Nat. Sci. Rev.*, **2020**, 7, 1726–1742
[18] T. Yutthalekha, D. Suttipat, S. Salakhum, A. Thivasasith, S. Nokbin, J. Limtrakul, C. Wattanakit, *Chem. Commun.*, **2017**, 53, 12185–12188.
[19] D. Verboekend, N. Nuttens, R. Locus, J. Van Aelst, P. Verolme, J. C. Groen, J. Perez-Ramirez, B. F. Sels, *Chem. Soc. Rev.*, **2016**, 45, 3331–3352.
[20] J. Van Aelst, D. Verboekend, A. Philippaerts, N. Nuttens, M. Kurttepeli, E. Gobechiya, M. Haouas, S. P. Sree, J. F. M. Denayer, J. A. Martens, C. E. A. Kirschhock, F. Taulelle, S. Bals, G. V. Baron, P. A. Jacobs, B. F. Sels, *Adv. Funct. Mater.*, **2015**, 25, 7130–7144.
[21] M. Gackowski, K. Tarach, L. Kuterasinski, J. Podobinski, S. Jarczewski, P. Kustrowski, J. Datka, *Microporous Mesoporous Mater.*, **2018**, 263, 282–288.
[22] K. X. Lee, J. A. Valla, *Appl. Catal. B*, **2017**, 201, 359–369.
[23] J. Kim, C. Jo, S. Lee, R. Ryoo, *J. Mater. Chem. A*, **2014**, 2, 11905–11912.
[24] M. Qamar, I. Baig, A. M. Azad, M. I. Ahmed, M. Qamaruddin, *Chem. Eng. J.*, **2016**, 290, 282–289.
[25] W. Q. Fu, L. Zhang, T. D. Tang, Q. P. Ke, S. Wang, J. B. Hu, G. Y. Fang, J. X. Li, F. S. Xiao, *J. Am. Chem. Soc.*, **2011**, 133, 15346–15349.
[26] C. H. L. Tempelman, X. C. Zhu, K. Gudun, B. Mezari, B. J. Shen, E. J. M. Hensen, *Fuel Process. Technol.*, **2015**, 139, 248–258.
[27] A. Inayat, I. Knoke, E. Spiecker, W. Schwieger, *Angew. Chem. Int. Ed.*, **2012**, 51, 1962–1965.
[28] J. Y. Wang, P. S. Liu, M. Boronat, P. Ferri, Z. G. Xu, P. Liu, B. J. Shen, Z. D. Wang, J. H. Yu, *Angew. Chem. Int. Ed.*, **2020**, 59, 17225–17228.
[29] M. D. Oleksiak, K. Muraoka, M. F. Hsieh, M. T. Conato, A. Shimojima, T. Okubo, W. Chaikittisilp, J. D. Rimer, *Angew. Chem. Int. Ed.*, **2017**, 56, 13366–13371.
[30] F. Delprato, L. Delmotte, J. L. Guth, L. Huve, *Zeolites*, **1990**, 10, 546–552.
[31] D. L. Zhu, L. Y. Wang, D. Fan, N. N. Yan, S. J. Huang, S. T. Xu, P. Guo, M. Yang, J. M. Zhang, P. Tian, Z. M. Liu, *Adv. Mater.*, **2020**, 32, 2000272.
[32] Q. Ke, I. Khalil, B. Smeyers, Z. Li, R. de Oliveira-Silva, B. Sels, D. Sakellariou, M. Dusselier, *Angew. Chem. Int. Ed.*, **2021**, 60, 24189–24197
[33] K. Fujii, S. Hayashi, H. Kodama, *Chem. Mater.*, **2003**, 15, 1189–1197.
[34] C. Wang, M. Yang, P. Tian, S. T. Xu, Y. Yang, D. H. Wang, Y. Y. Yuan, Z. M. Liu, *J. Mater. Chem. A*, **2015**, 3, 5608–5616.
[35] L. Peng, X. H. Xu, X. Yao, H. Liu, X. H. Gu, *J. Membr. Sci.*, **2018**, 549, 446–455.
[36] A. Shimojima, Y. Sugahara, K. Kuroda, *Bull. Chem. Soc. Jpn.*, **1997**, 70, 2847–2853.
[37] H. Xu, C. Lei, Q. M. Wu, Q. Y. Zhu, X. J. Meng, D. N. Dai, S. Maurer, A. N. Parvulescu, U. M?ller, F. S. Xiao, *Front. Chem. Sci. Eng.*, **2020**, 14, 267–274.
[38] J. Li, J. Qiu, Y. J. Sun, Y. C. Long, *Microporous Mesoporous Mater.*, **2000**, 37, 365–378.
[39] J. Zhu, Y. H. Zhu, L. K. Zhu, M. Rigutto, A. van der Made, C. G. Yang, S. X. Pan, L. Wang, L. F. Zhu, Y. Y. Jin, Q. Sun, Q. M. Wu, X. J. Meng, D. L. Zhang, Y. Han, J. X. Li, Y. Y. Chu, A. M. Zheng, S. L. Qiu, X. M. Zheng, F. S. Xiao, *J. Am. Chem. Soc.*, **2014**, 136, 2503–2510.
[40] C. Wang, M. Yang, M. R. Li, S. T. Xu, Y. Yang, P. Tian, Z. M. Liu, *Chem. Commun.*, **2016**, 52, 6463–6466.
[41] M. Choi, K. Na, J. Kim, Y. Sakamoto, O. Terasaki, R. Ryoo, *Nature*, **2009**, 461, 246–249.
[42] Z. Qin, L. Lakiss, J. P. Gilson, K. Thomas, J. M. Goupil, C. Fernandez, V. Valtchev, *Chem. Mater.*, **2013**, 25, 2759–2766.
[43] D. P. Serrano, J. Aguado, G. Morales, J. M. Rodriguez, A. Peral, M. Thommes, J. D. Epping, B. F. Chmelka, *Chem. Mater.*, **2009**, 21, 641–654.

[44] C. A. Emeis, *J. Catal.*, **1993**, 141, 347–354.
[45] D. P. Serrano, R. A. Garcia, G. Vicente, M. Linares, D. Prochazkova, J. Cejka, *J. Catal.*, **2011**, 279, 366–380.
[46] C. Flego, I. Kiricsi, C. Perego, G. Bellussi, *Catal. Lett.*, **1995**, 35, 125–133.
[47] M. Maache, A. Janin, J. C. Lavalley, J. F. Joly, E. Benazzi, *Zeolites*, **1993**, 13, 419–426.
[48] B. Shirani, X. Han, M. Eic, *Sep. Purif. Technol.*, **2020**, 230, 115831.

介孔高硅Y沸石的合成及催化裂化性能

崔文浩[a,b,†], 朱大丽[a,b,†], 谭 涓[c], 陈 南[a,b], 樊 栋[a], 王 娟[a], 韩晶峰[a], 王林英[a,*], 田 鹏[a,#], 刘中民[a]

[a]中国科学院大连化学物理研究所, 洁净能源国家实验室(筹), 甲醇制烯烃国家工程实验室, 辽宁大连116023
[b]中国科学院大学, 北京100049
[c]大连理工大学化工与环境生命学部, 化学工程学院, 催化化学与工程系, 辽宁大连116024

摘要: Y型沸石拥有三维十二元环孔道(孔径0.74 nm)以及超笼结构(直径1.12 nm), 在石油冶炼、石油加工、精细化学品合成以及新兴生物油的炼制方面具有重要应用. 研究表明, 随着Y沸石骨架硅铝比(SiO_2/Al_2O_3, 简称SAR)提高, 酸中心强度增加, 酸密度降低, 有助于抑制裂化反应中积碳导致催化剂的失活, 并提高催化剂活性; 另外, 随着沸石骨架硅铝比提高, Y沸石对应热/水热稳定性相应增加, 有利于保持催化剂长周期使用性能. Y沸石的大孔结构使其在工业应用中有着显著的优势, 然而对于大分子反应物, 反应物与沸石内部活性位点的接触以及相应的产物扩散仍限制了其催化性能. 介孔沸石同时具有微孔和介孔两类孔道结构, 可以克服微孔沸石有限孔径尺寸带来的传质限制, 进一步提高反应性能. 现在工业上应用的高硅Y沸石均是通过酸脱铝, 水蒸汽辅助脱铝等后处理方法获得. 虽然后处理过程可以提高沸石骨架硅铝比, 并引入适量的介孔结构, 改善其在催化裂化反应中的传质性能, 但后处理过程工序复杂, 耗时耗能, 而且会形成脱铝梯度, 不利于其催化应用. 相对而言, 直接合成介孔高硅Y沸石是最理想的途径.

本文以商用双亲性有机硅烷作为介孔模板剂, 采用晶核、有机模板剂与低碱度协同作用(NOA-co)策略一步直接合成介孔高硅Y沸石(MSY). 研究了投料硅铝比、介孔剂加入量以及加入顺序对催化性能的影响. 实验发现, 产品的介孔孔容、外比表面积以及SAR随着介孔剂加入量的增加而逐渐提高, 当介孔剂添加过量时无法得到纯相. 合成的介孔高硅Y沸石具有高SAR(9.8–12.6)和介孔孔容(0.13–0.22 cm^3/g). 选取SAR = 10.7的介孔高硅Y沸石样品($MSY_{10.7}$)进行进一步研究. 扫描电镜及透射电镜结果表明, MSY沸石具有典型八面体形貌、丰富的晶内介孔及优异的热/水热稳定性, 晶粒中铝分布均匀. 与商用USY沸石相比, MSY沸石具有更多的强酸中心和更高的酸强度. 选取大分子1,3,5-三异丙基苯的催化裂化反应探究其催化性能. H-$MSY_{10.7}$样品因具有大的外比表面积和丰富的酸性位点, 在1,3,5-三异丙基苯催化裂化反应中表现出高的催化活性、最慢的失活速率及最高的裂解深度. 进一步研究了MSY沸石在工业重油裂化反应中的催化性能. 以La改性的$MSY_{10.7}$为活性组分, 采用催化裂化催化剂制备方法制备了所需催化剂, 经800 °C高温老化处理后, $MSY_{10.7}$基催化剂的催化性能较工业流化催化裂化(FCC)催化剂转化率提高了7.64%, 汽油收率提高了16.37%. 综上, 本文一步法制备的介孔高硅Y沸石具有优异的大分子裂化性能, 为工业催化裂化催化剂的制备和性能提升提供了新方法新思路.

关键词: 介孔沸石; FAU; 合成; 高硅Y沸石; 流化催化裂化

收稿日期: 2021-12-06. 接受日期: 2022-03-02. 上网时间: 2022-05-20.
*通讯联系人. 电子信箱: lywang@dicp.ac.cn
#通讯联系人. 电子信箱: tianpeng@dicp.ac.cn
†共同第一作者.
基金来源: 国家自然科学基金(21991090, 21991091); 中国科学院前沿科学重点研究项目(QYZDB-SSW-JSC040); 中科院大连化学物理研究所自主部署基金(DICP ZZBS201807).
本文的电子版全文由Elsevier出版社在ScienceDirect上出版(http://www.sciencedirect.com/journal/chinese-journal-of-catalysis).